Earthq Eng & Eng Vib (2021) 20: 1021-1032 **DOI**: https://doi.org/10.1007/s11803-021-2066-z

Optimal design and effectiveness evaluation for inerter-based devices on mitigating seismic responses of base isolated structures

Li Yafeng†, Li Shouying‡ and Chen Zhengqing‡

Key Laboratory for Wind and Bridge Engineering of Hunan Province, College of Civil Engineering, Hunan University, Changsha 410082, China

Abstract: The optimal design and effectiveness of three control systems, tuned viscous mass damper (TVMD), tuned inerter damper (TID) and tuned mass damper (TMD), on mitigating the seismic responses of base isolated structures, were systematically studied. First, the seismic responses of the base isolated structure with each control system under white noise excitation were obtained. Then, the structural parameter optimizations of the TVMD, TID and TMD were conducted by using three different objectives. The results show that the three control systems were all effective in minimizing the root mean square value of seismic responses, including the base shear of the BIS, the absolute acceleration of structural SDOF, and the relative displacement between the base isolation floor and the foundation. Finally, considering the superstructure as a structural MDOF, a series of time history analyses were performed to investigate the effectiveness and activation sensitivity of the three control systems under far field and near fault seismic excitations. The results show that the effectiveness of TID and TMD with optimized parameters on mitigating the seismic responses of base isolated structures increased as the mass ratio increases, and the effectiveness of TID was always better than TMD with the same mass ratio. The TVMD with a lower mass ratio was more efficient in reducing the seismic response than the TID and TMD. Furthermore, the TVMD, when compared with TMD and TID, had better activation sensitivity and a smaller stroke.

Keywords: base isolated structure; inerter; optimal design; seismic response; vibration control

1 Introduction

Base isolations have become one of the most effective countermeasures for seismic fortification of civil structures (Nepal and Saitoh, 2020; Peng *et al*., 2020; Walsh and Abdullah, 2006; Satish and Anil, 2017; Xue *et al*., 2019). By installing isolation devices (such as rubber bearings) with small lateral stiffness between a superstructure and its foundation, the period of the first mode of the superstructure can be lengthened, and thereby reducing the earthquake energy input to the superstructure. For a base isolated structure (BIS), relative displacement induced by earthquakes between the base isolation floor and the foundation is significant, and the superstructure behaves almost as a rigid body (Xiang and Nishitani, 2014; De and Ricciardi, 2018a). This relative displacement should be carefully restricted to avoid collision damage between the base isolation floor and surrounding structures or piping components. To reduce the relative displacement between the base isolation floor and the foundation, energy dissipation devices, for example viscous dampers, were usually added between the base isolation floor and the foundation (Qiu and Tian, 2018; Ryan and Polanco, 2008). However, these energy dissipation devices have an unexpected effect on increasing the absolute acceleration of the superstructure (Jangid and Banerji, 1998; Kelly, 1999; Lee and Kelly, 2019).

The use of base isolations on high-rise buildings was often restricted by the overturning effect. Excessive overturning moment at the base of the BIS may cause a dramatic change in the axial force of the isolation bearings and may even push some of them into a tensioned state (Lu *et al*., 2016). This shortcoming of base isolation on high-rise buildings can be overcome by using a "hybrid" control strategy, which combines conventional base isolation with other vibration control systems (Yang *et al*., 1991; Adam *et al*., 2017). For example, the tuned mass damper (TMD) (Rezazadeh *et al*., 2020), a common passive vibration control system, can be used to reduce the overturning moment of base

Correspondence to: Li Shouying, Key Laboratory for Wind and Bridge Engineering of Hunan Province, College of Civil Engineering, Hunan University, Changsha 410082, China
Tel: +86-13975197401; Fax: +86-731-88823923
E-mail: shyli@hnu.edu.cn
†Graduate Student; ‡Professor

Supported by: National Key Research and Development Program of China under Grant No. 2017YFC0703600 and No. 2017YFC0703604
Received July 12, 2020; **Accepted** March 9, 2021

isolated structures. However, TMDs may not be a good choice due to its stroke limitation and large mass ratio requirement (Taniguchi *et al*., 2008; Xiang and Nishitani, 2014).

In the latest twenty years, inerter-based devices have been developed and adopted to mitigate the vibrations of civil structures. In 1973, Kawamata (1973) first proposed a two-terminal mass enhancement device, which was the first application of an inerter in the engineering field. The concept of the inerter was not proposed until 2002 (Smith, 2002). It is a two-node mechanical element, in which the output force between the two nodes is proportional to the relative acceleration. The proportional coefficient is called an inertance (Chen *et al*., 2014; Hu and Chen, 2015). More importantly, the value of inertance can be many times larger than the physical mass by using some special devices, such as rack-gear (Smith, 2002; Li *et al*., 2020a, 2020b), ball-screw (Papageorgiou and Smith, 2005) or helical-tube fluid (Liu *et al*., 2018).

The inerter provides a novel tool to reduce harmful vibrations. Arai *et al*. (2009) and Ikago *et al*. (2012) developed a tuned viscous mass damper (TVMD) and the optimization of its parameters was systematically performed. Huang *et al*. (2019) extended the optimal design of the TVMD with a nonlinear viscous damper for a single-degree-of-freedom (SDOF) system. Zhang *et al*. (2020) theoretically discovered the damping enhancement effect of TVMD and proposed a universal design principle for it. Lazar *et al*. (2014) proposed a tuned inerter damper (TID), and numerical simulations on a multi-story building subjected to base excitation were carried out to verify its efficiency. Wen *et al*. (2016) further compared the effectiveness of TVMD and TID in reducing the seismic-induced vibrations of multi-degree-of-freedom (MDOF) structures. Marian and Giaralis (2014; 2017) proposed a novel tuned mass damper inerter (TMDI) by adding an inerter between the TMD and the foundation, and the optimization of the TMDI was conducted. After that, a series of studies were performed to examine the effectiveness of the TMDI when subjected to earthquakes (Pietrosanti *et al*., 2017; De and Ricciardi, 2018a) and wind (Giaralis and Petrini, 2017; Xu *et al*., 2019).

In recent years, the inerter has been gradually used in the BIS. Hashimoto *et al*. (2015) investigated the effect of the inerter on TMD stroke for BIS with large mass ratio. De and Ricciardi (2018a; 2018b) proposed an enhanced BIS incorporating the TMDI by considering the linearity and nonlinearity of the isolators. The effectiveness of the TMDI was compared with the conventional TMD. Sun *et al*. (2019) and Ye *et al*. (2019) obtained closed-form solutions for base isolated structures equipped with TID and additional inertia, respectively. Zhao *et al*. (2019a; 2019b) compared the performances of TMD and TVMD based on BIS with a friction pendulum bearing. The previous studies demonstrated that TVMD and TID are effective in mitigating the relative displacement between the base isolation floor and the foundation. However, the effects of the TVMD or TID on the overturning effect of the BIS have seldom been studied. In addition, the activation sensitivity of the TVMD and TID under different types of earthquakes has not been elucidated.

In this study, the effects of three control systems (TVMD, TID and TMD) combined with base isolation on the responses of the superstructure, including the base shear, base overturning moment, and the relative displacement between the base isolation floor and the foundation, were systematically studied. First, the seismic responses of BIS with each control system under white noise excitation were obtained. Then, the optimal designs of the TVMD, TID and TMD were carried out by using three different objectives, and the dynamic responses of the BIS in terms of root mean square values were comprehensively investigated. Finally, by considering the superstructure as a structural MDOF, a series of time history analyses were performed to investigate the effectiveness and activation sensitivity of the three control systems under far field and near fault seismic excitations.

2 Theoretical model

2.1 Mechanical model for base isolated structure with three control systems

A base isolated structure, which consists of a single-degree-of-freedom superstructure (structural SDOF) and base isolation floor, is schematically shown in Fig. 1. A control system is arranged between the base isolation floor and the foundation. The structural SDOF, which has a mass of m_s, a linear stiffness of k_s and a viscous damping coefficient of c_s, can be obtained from a multi-degree-of-freedom superstructure (structural MDOF) based on its first mode. The relative displacement between the structural SDOF and the foundation is represented by x_s. m_b is the mass of the base isolation floor, and k_b and c_b are, respectively, the linear stiffness and the viscous damping coefficient of the isolation bearings. The relative displacement between the base isolation floor and the foundation is represented by x_b. Three types of control systems, the TVMD, TID and TMD, are taken into account and shown in Fig. 1. b_t is the inertance for TVMD and TID, and m_t is the physical mass for TMD. k_t and c_t are the linear stiffness and the viscous damping coefficient of three control systems, respectively, and x_t represents the stroke of the control systems relative to the foundation. $\ddot{x}_g$ is the ground acceleration of earthquake. Therefore, the base isolated structure with control system can be described by three degree-of-freedoms, x_s, x_b and x_t as shown in Fig. 1.

2.2 Motion equations

It is more convenient to derive the motion equations of the BIS with each control system by using a relative

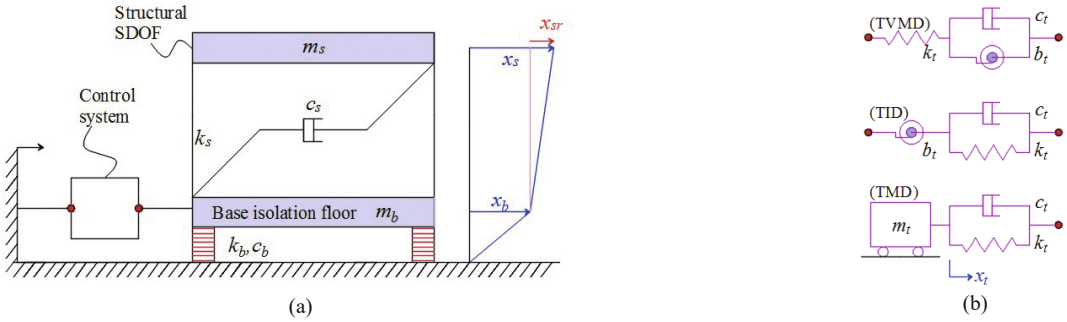

Fig. 1 Base isolated structure with control systems

displacement $x_{sr}=x_s-x_b$ (as shown in Fig. 1) instead of x_s. Based on the d'Alembert's Principle, the equations governing the motion of the 3-DOF system in Fig. 1 can be written as,

$$\ddot{x}_{sr}+\ddot{x}_b+2\xi_s\omega_s\dot{x}_{sr}+\omega_s^{\,2}x_{sr}=-\ddot{x}_g \tag{1}$$

$$\begin{aligned}&\mu_b\ddot{x}_b+2\mu_b\xi_b\omega_b\dot{x}_b+\mu_b\omega_b^{\,2}x_b-\\&2\xi_s\omega_s\dot{x}_{sr}-\omega_s^{\,2}x_{sr}+\frac{f_c}{m_s}=-\mu_b\ddot{x}_g\end{aligned} \tag{2}$$

in which,

$$\frac{f_{\text{c-TVMD}}}{m_s}=\beta_t\left(\ddot{x}_b-\ddot{x}_t\right)+2\xi_t\omega_s\left(\dot{x}_b-\dot{x}_t\right)=\omega_s^{\,2}\eta_t x_t \tag{3a}$$

$$\frac{f_{\text{c-TID}}}{m_s}=2\xi_t\omega_s\left(\dot{x}_b-\dot{x}_t\right)+\omega_s^{\,2}\eta_t\left(x_b-x_t\right)=\beta_t\ddot{x}_t \tag{3b}$$

$$\frac{f_{\text{c-TMD}}}{m_s}=2\xi_t\omega_s\left(\dot{x}_b-\dot{x}_t\right)+\omega_s^{\,2}\eta_t\left(x_b-x_t\right)-\beta_t\ddot{x}_g=\beta_t\ddot{x}_t \tag{3c}$$

where, f_c represents the output force of the control systems; $f_{\text{c-TVMD}}$, $f_{\text{c-TID}}$ and $f_{\text{c-TMD}}$, respectively, correspond to the output forces of the TVMD, TID and TMD.

In Eqs. (1)–(3), the following parameters are introduced,

$$\begin{aligned}&\omega_s=\sqrt{\frac{k_s}{m_s}},\xi_s=\frac{c_s}{2m_s\omega_s},\\&\omega_b=\sqrt{\frac{k_b}{m_b}},\xi_b=\frac{c_b}{2m_b\omega_b},\mu_b=\frac{m_b}{m_s}\end{aligned} \tag{4a}$$

$$\begin{aligned}&\beta_t=\frac{b_t}{m_s}\left(\text{for TVMD and TID}\right)\text{or}\ \frac{m_t}{m_s}\left(\text{for TMD}\right),\\&\eta_t=\frac{k_t}{k_s},\xi_t=\frac{c_t}{2m_s\omega_s}\end{aligned} \tag{4b}$$

The parameters in Eq. (4a) are related to the BIS, including the natural frequency ω_s and the damping ratio ξ_s of the structural SDOF, the natural frequency ω_b and the damping ratio ξ_b of the base isolation floor and the mass ratio μ_b. The parameters in Eq. (4b) are related to the control systems, including the inertance-mass ratio β_t for TVMD and TID or the physical mass ratio β_t for TMD, the linear stiffness ratio η_t and the viscous damping ratio ξ_t.

2.3 Seismic response under white noise excitation

In consideration of the uncertain property of earthquakes, it is reasonable for the structural design to assume the ground acceleration excitation $\ddot{x}_g$ as a Gaussian white noise random process, which is characterized by its power spectral density $S_{\ddot{x}_g}=S_0$. Transforming Eqs. (1)–(3) into the first-order state space form,

$$\dot{\boldsymbol{z}}(t)=\boldsymbol{A}\boldsymbol{z}(t)+\boldsymbol{B}\ddot{x}_g \tag{5}$$

in which, $\boldsymbol{z}(t)=(x_{sr}\ x_b\ x_t\ \dot{x}_{sr}\ \dot{x}_b\ \dot{x}_t)^{\mathrm{T}}$ is the state vector; $\boldsymbol{A}$ is the state matrix; and $\boldsymbol{B}$ is the input vector. The state matrix $\boldsymbol{A}$ and the input vector $\boldsymbol{B}$ corresponding to three types of control systems, $\boldsymbol{A}_{\text{c-TVMD}}$, $\boldsymbol{A}_{\text{c-TID}}$, $\boldsymbol{A}_{\text{c-TMD}}$, $\boldsymbol{B}_{\text{c-TVMD}}$, $\boldsymbol{B}_{\text{c-TID}}$ and $\boldsymbol{B}_{\text{c-TMD}}$ can be written as,

$$\boldsymbol{A}_{\text{c-TVMD}}=\begin{bmatrix}0&0&0&1&0&0\\0&0&0&0&1&0\\0&0&0&0&0&1\\-\alpha_1-\omega_s^{\,2}&\alpha_2&\alpha_3&-(\alpha_4+\mu_b\alpha_4)&\alpha_5&0\\\alpha_1&-\alpha_2&-\alpha_3&\alpha_4&-\alpha_5&0\\\alpha_1&-\alpha_2&-\left(\alpha_3+\alpha_3\dfrac{\mu_b}{\beta_t}\right)&\alpha_4&\alpha_6-\alpha_5&-\alpha_6\end{bmatrix},$$

$$\boldsymbol{B}_{\text{c-TVMD}}=\begin{bmatrix}0\\0\\0\\0\\-1\\-1\end{bmatrix} \tag{6a}$$

$$\boldsymbol{A}_{\text{c-TID}}=\begin{bmatrix} 0 & 0 & 0 & 1 & 0 & 0 \\ 0 & 0 & 0 & 0 & 1 & 0 \\ 0 & 0 & 0 & 0 & 0 & 1 \\ -\alpha_1-\omega_s^2 & \alpha_2+\alpha_3 & -\alpha_3 & -(\alpha_4+\mu_b\alpha_4) & \alpha_5+\alpha_7 & -\alpha_7 \\ \alpha_1 & -(\alpha_2+\alpha_3) & \alpha_3 & \alpha_4 & -(\alpha_5+\alpha_7) & \alpha_7 \\ 0 & \alpha_3\dfrac{\mu_b}{\beta_t} & -\alpha_3\dfrac{\mu_b}{\beta_t} & 0 & \alpha_6 & -\alpha_6 \end{bmatrix},$$

$$\boldsymbol{B}_{\text{c-TID}}=\begin{bmatrix} 0 \\ 0 \\ 0 \\ 0 \\ -1 \\ 0 \end{bmatrix} \tag{6b}$$

$$\boldsymbol{A}_{\text{c-TMD}}=\boldsymbol{A}_{\text{c-TID}},\ \boldsymbol{B}_{\text{c-TMD}}=\begin{bmatrix} 0 \\ 0 \\ 0 \\ 0 \\ -1 \\ -1 \end{bmatrix} \tag{6c}$$

where,

$$\begin{cases} \alpha_1=\dfrac{1}{\mu_b}\omega_s^{\,2},\ \alpha_2=\omega_b^{\,2},\ \alpha_3=\dfrac{1}{\mu_b}\omega_s^{\,2}\eta_t,\ \alpha_4=2\dfrac{1}{\mu_b}\xi_s\omega_s \\ \alpha_5=2\xi_b\omega_b,\ \alpha_6=2\dfrac{1}{\beta_t}\xi_t\omega_s,\ \alpha_7=\alpha_6\dfrac{\beta_t}{\mu_b} \end{cases} \tag{7}$$

The covariance matrix $\boldsymbol{G}_{zz}$ for the complete description of the response $\boldsymbol{z}(t)$ can be expressed as,

$$\boldsymbol{G}_{zz}=E\left[\boldsymbol{z}(t)\cdot\boldsymbol{z}(t)^{\mathrm{T}}\right] \tag{8}$$

in which, the symbol $E[\cdot]$ represents the expected value operator. The covariance matrix $\boldsymbol{G}_{zz}$ satisfies the Lyapunov equation (Pietrosanti *et al*., 2017),

$$\boldsymbol{A}\boldsymbol{G}_{zz}+\boldsymbol{G}_{zz}\boldsymbol{A}^{\mathrm{T}}+2\pi S_0\boldsymbol{B}\boldsymbol{B}^{\mathrm{T}}=0 \tag{9}$$

By using Eq. (1), the absolute acceleration of structure SDOF $\ddot{x}_a$ can be defined as,

$$\ddot{x}_a=\ddot{x}_{sr}+\ddot{x}_b+\ddot{x}_g=-2\xi_s\omega_s\dot{x}_{sr}-\omega_s^{\,2}x_{sr} \tag{10}$$

By solving Eq. (9) numerically, it is convenient to obtain the following response,

$$\begin{aligned}\sigma_a^2&=E\left[\ddot{x}_a^{\,2}\right]=E\left[\left(\ddot{x}_{sr}+\ddot{x}_b+\ddot{x}_g\right)^2\right] \\ &=4\xi_s^{\,2}\omega_s^{\,2}E\left(\dot{x}_{sr}^{\,2}\right)+\omega_s^{\,4}E\left(x_{sr}^{\,2}\right)\end{aligned} \tag{11}$$

$$\sigma_{xb}^2=E\left[x_b^{\,2}\right] \tag{12}$$

where σ_a and σ_{xb} denote the root mean square (RMS) of absolute acceleration of structural SDOF and the RMS of relative displacement between the base isolation floor and the foundation, respectively.

The RMS of the base shear σ_f of the base isolated structure with the control of TVMD, TID and TMD can be obtained by Eqs. (13a), (13b) and (13c), respectively, as follows,

$$\begin{aligned}&\sigma_f^2=m_s^2\sigma_a^2+m_b^2\cdot \\ &\left[\begin{aligned}&-\alpha_1^2E\left(x_{sr}^2\right)+\alpha_2^2E\left(x_b^2\right)+\alpha_3^2E\left(x_t^2\right)-\alpha_4^2E\left(\dot{x}_{sr}^2\right)+\alpha_5^2E\left(\dot{x}_b^2\right) \\ &+2\alpha_2\alpha_3E\left(x_bx_t\right)+2\alpha_3\alpha_5E\left(x_t\dot{x}_b\right)\end{aligned}\right]\end{aligned} \tag{13a}$$

$$\begin{aligned}&\sigma_f^2=m_s^2\sigma_a^2+m_b^2\cdot \\ &\left[\begin{aligned}&-\alpha_1^2E\left(x_{sr}^2\right)+(\alpha_2+\alpha_3)^2E\left(x_b^2\right)+\alpha_3^2E\left(x_t^2\right)-\alpha_4^2E\left(\dot{x}_{sr}^2\right)+(\alpha_5+\alpha_7)^2E\left(\dot{x}_b^2\right) \\ &+\alpha_7^2E\left(\dot{x}_t^2\right)-2(\alpha_2+\alpha_3)\left[\alpha_3E\left(x_bx_t\right)+\alpha_7E\left(x_b\dot{x}_t\right)\right] \\ &-2(\alpha_5+\alpha_7)\left[\alpha_3E\left(\dot{x}_bx_t\right)+\alpha_7E\left(\dot{x}_b\dot{x}_t\right)\right]\end{aligned}\right]\end{aligned} \tag{13b}$$

$$\begin{aligned}&\sigma_f^2=m_s^2\sigma_a^2+m_b^2\cdot \\ &\left[\begin{aligned}&-\alpha_1^2E\left(x_{sr}^2\right)+(\alpha_2+\alpha_3)^2E\left(x_b^2\right)+\alpha_3^2E\left(x_t^2\right)-\alpha_4^2E\left(\dot{x}_{sr}^2\right)+(\alpha_5+\alpha_7)^2E\left(\dot{x}_b^2\right) \\ &+\alpha_7^2E\left(\dot{x}_t^2\right)-2(\alpha_2+\alpha_3)\left[\alpha_3E\left(x_bx_t\right)+\alpha_7E\left(x_b\dot{x}_t\right)\right] \\ &-2(\alpha_5+\alpha_7)\left[\alpha_3E\left(\dot{x}_bx_t\right)+\alpha_7E\left(\dot{x}_b\dot{x}_t\right)\right]\end{aligned}\right]\end{aligned} \tag{13c}$$

For base isolated structure without a control system, the same method is used to obtain the RMS of the absolute acceleration of the structure SDOF (σ_{a0}), the RMS of displacement of the base isolation floor (σ_{xb0}) and the RMS of the base shear (σ_{f0}) by letting f_c in Eq. (2) to be equal to 0.

3 Optimization of structural parameters for the control systems

3.1 Possible objectives

In this section, a structural SDOF model simplified from a seven-story MDOF building which has been used in previous studies (Nakaminami *et al*., 2011; Zhao *et al*., 2019b) was adopted as an example for numerical simulations, as shown in Table 1. There are eight structural parameters in the motion equations of the BIS with a control system, which are shown in Eq. (4). Three of them, including ω_s, ω_b and μ_b, can be directly calculated from the data listed in Table 1,

$$\omega_s=7.54,\quad \omega_b=3.31,\quad \mu_b=0.29 \tag{14a}$$

The damping ratios of the superstructure and the base isolation floor, ζ_s and ζ_b, can be approximately given as follows (De and Ricciardi, 2018a),

Table 1 Model information of structural MDOF and structural SDOF

Story	Structural MDOF			Structural SDOF		
	Mass (ton)	Stiffness (kN/m)	Height (m)	Mass (ton)	Stiffness (kN/m)	Height (m)
7	1,039	1,475,900	4.70	21,015	1,195,770	—
6	3,897	3,143,400	3.80			
5	3,477	4,581,300	3.80			
4	3,600	4,976,600	3.80			
3	3,615	3,877,500	4.40			
2	3,856	4,075,700	4.40			
1	4,671	3,519,300	5.45			
Base isolation floor	6,115	66,940	0.10	6,115	66,940	0.10
Total	30,269		30.45	27,130	—	—

$$\zeta_s = 0.02, \quad \zeta_b = 0.10 \tag{14b}$$

As for the other three structural parameters related to the control systems, including β_t, η_t and ξ_t, their optimal values should be determined by a series of design optimizations. First, β_t is given an appropriate value (0.05–0.7), then η_t and ζ_t are changed with increments of 10^{-4} to obtain the desired accuracy within the ranges as follows,

$$0.0001 \le \eta_t \le 0.5, \quad 0.0001 \le \xi_t \le 0.5 \tag{15}$$

Three different design objectives were considered to understand how the optimal structural parameters of the three control systems will change. The three design objectives are to minimize the RMS of base shear of BIS, minimize the RMS of absolute acceleration of structural SDOF, and minimize the RMS of relative displacement between the base isolation floor and the foundation, respectively. For comparison purposes, three values, I_f, I_a, I_d, corresponding to three different design objectives are normalized with respect to the uncontrolled situation as,

$$I_f = \frac{\sigma_f}{\sigma_{f0}}, \; I_a = \frac{\sigma_a}{\sigma_{a0}}, \; I_d = \frac{\sigma_{xb}}{\sigma_{xb0}} \tag{16}$$

3.2 Minimization of the base shear of the BIS

Figure 2(a) presents the variation of objective I_f with the mass ratio β_t for the three types of control systems (TVMD, TID and TMD), and Figs. 2(b)–2(c) show the corresponding optimal structural parameters η_{topt} and ξ_{topt}. It can be found from Fig. 2(a) that all values of I_f are less than 1.0, which means that the three types of control systems are effective in minimizing the base shear of the BIS. It appears that the best performance can be obtained for the BIS by using the TVMD when the mass ratio β_t is less than 0.45. More importantly, it seems that the smallest mass ratio (β_t=0.05) can make the TVMD more efficient.

For both the TID and the TMD, it can be found from Fig. 2(a) that their effectiveness on mitigating the base shear of the BIS increases with the increase of the mass ratio β_t. The effectiveness of the TID is apparently better than the TMD with the same mass ratio β_t, and the results confirm others obtained in previous studies (Pietrosanti *et al*., 2017). Note that a large mass ratio β_t for the TMD is unreasonable for economic considerations.

From Figs. 2(b) and 2(c), it can be found that the values of η_{topt} and ξ_{topt} of the TVMD are far greater than those of the TID and the TMD in all cases of the mass ratio β_t. It appears that the η_{topt} and ξ_{topt} of the TID and the TMD show an approximate linear growth trend with the increase of the mass ratio β_t, while the variations of η_{topt} and ξ_{topt} for the TVMD have considerable uncertainty.

3.3 Minimization of the absolute acceleration of the structural SDOF

Figure 3 presents the objective I_a with the mass ratio β_t, together with the corresponding optimal structural parameters η_{topt} and ξ_{topt} for the three types of control systems. It can be found from Fig. 3(a) that the objective I_a are all lower than 1.0, which indicates that the three control systems are effective in reducing the absolute acceleration of the structural SDOF. In addition, it appears that the objective I_a in Fig. 3(a) is very close to the corresponding objective I_f in Fig. 2(a). This is because the base shear of the BIS has a close relationship with the absolute acceleration of the structural SDOF, as shown in Eq. (13).

It can be found from Fig. 3 that the optimal structural parameters η_{topt} and ξ_{topt} of the TID and the TMD are also close to the corresponding results in Fig. 2. While the values of η_{topt} and ξ_{topt} of the TVMD in Fig. 3 are significantly lower than the corresponding results in Fig. 2 when β_t>0.15. Furthermore, there is a sudden drop for the η_{topt} and ξ_{topt} of the TVMD when 0.125<β_t<0.15, which is not seen in Fig. 2.

3.4 Minimization of the relative displacement between base isolation floor and foundation

Figure 4 presents the objective I_d and corresponding optimal structural parameters η_{topt} and ξ_{topt} for the three control systems. It can be found from Fig. 4 that the optimal values of η_{topt} and ξ_{topt} of the TID are almost equal to those of the TMD for the same mass ratio. However, the effectiveness of the TID and the TMD represented by objective index I_d gradually shows a gap with the increase of mass ratio β_t, and TID shows better performance than TMD with the same mass ratio β_t. Compared with the TID and the TMD, the TVMD is more efficient in reducing the relative displacement between the base isolation floor and the foundation. Note that the optimal values of η_{topt} and ξ_{topt} of the TVMD appear at the highest boundary 0.5 in all cases of the mass ratio β_t. These results can be seen in previous studies (Zhao *et al*., 2019b). This is predictable, because if the stiffness k_t and damping coefficient c_t of the TVMD are both infinite, the BIS with the TVMD is equivalent to a non-isolated structure. This indicates that there are no optimal structural parameters of η_{topt} and ξ_{topt} to minimize the RMS of the relative displacement between the base isolation floor and the foundation for the TVMD.

Figure 5(a) presents the objective I_d obtained by substituting η_{topt} and ξ_{topt} in Fig. 2 into Eqs. (12) and (16), and Fig. 5(b) presents the results obtained by substituting η_{topt} and ξ_{topt} in Fig. 3 into Eqs. (12) and (16). It can be found from Fig. 5 that the TVMD still has the best performance.

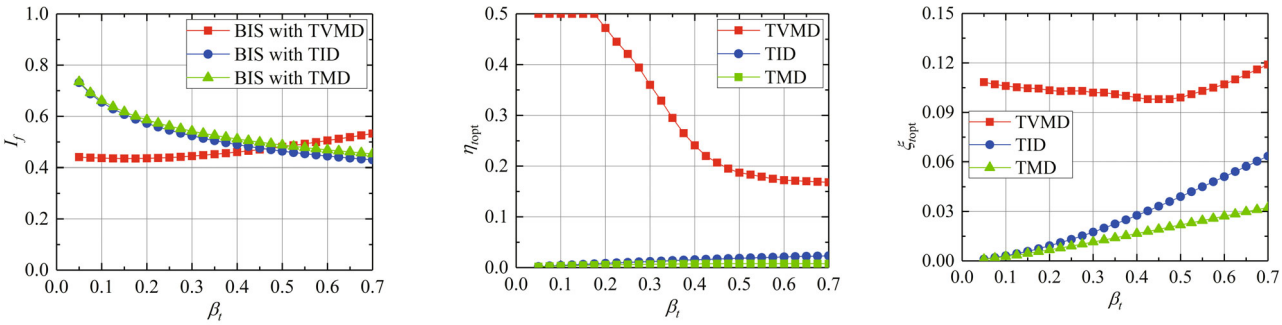

(a) Objective I_f (b) Values of η_{topt} (c) Values of ξ_{topt}

Fig. 2 Objective I_f and corresponding optimal structural parameters η_{topt} and ξ_{topt}

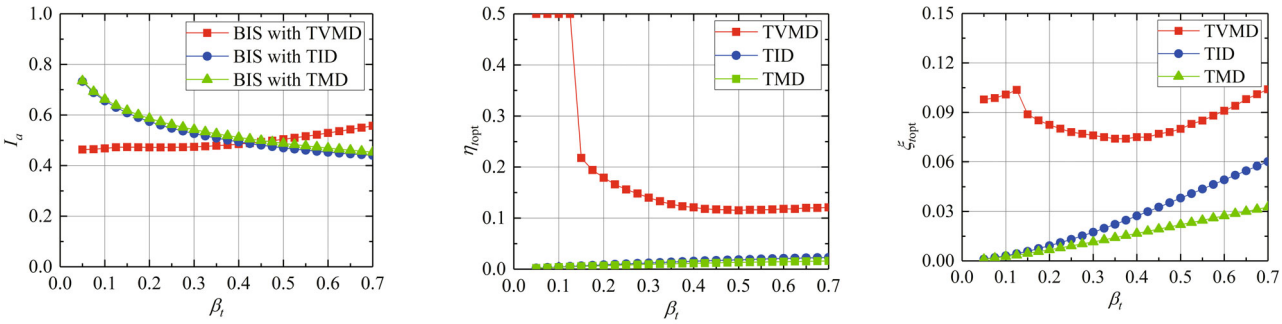

(a) Objective I_a (b) Values of η_{topt} (c) Values of ξ_{topt}

Fig. 3 Objective I_a and corresponding optimal structural parameters η_{topt} and ξ_{topt}

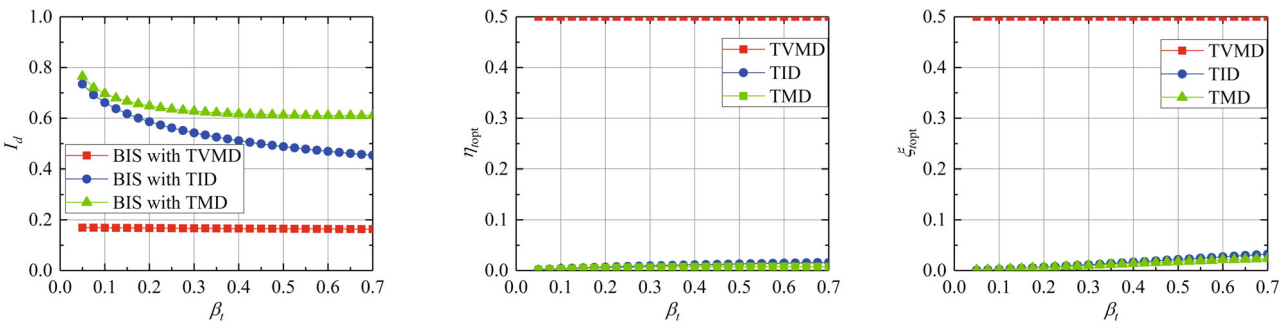

(a) Objective I_d (b) Values of η_{topt} (c) Values of ξ_{topt}

Fig. 4 Objective I_d and corresponding optimal structural parameters η_{topt} and ξ_{topt}

4 Seismic effectiveness verification

4.1 Parameters for numerical simulations

To investigate the effectiveness of the three control systems under natural seismic excitations, the structural MDOF model introduced in Table 1 was adopted to carry out time history analyses. The values of the structural parameters for the BIS are the same as those in Eqs. (14a) and (14b). The structural parameters of the three control systems were determined based on the optimization analysis in Section 3. Two typical earthquake records, as shown in Table 2, were used as ground motions in the numerical simulations, and each record contained a far field earthquake and a near fault earthquake, which were measured at different stations. These data were downloaded from the Peer Ground Motion Database. In order to keep the comparisons between different records at the same level, the peak accelerations of these natural earthquake records were all scaled to 0.3 g. Figure 6 presents the acceleration spectrums and velocity spectrums of these natural earthquake records with a damping ratio of 5%. It can be seen from Table 2 and Fig. 6 that near fault ground motions have obvious long-period velocity pulses.

4.2 Seismic responses of the structural MDOF

Four types of seismic responses, including the base shear f, base overturning moment M, the relative displacement between the base isolation floor and the foundation x_b and the stroke of control systems x_t, are specifically discussed to evaluate the effectiveness of the three control systems. For intuitive comparison, the performance indices $\tilde{I}_i$ and I_i (i = 1, 2, 3 and 4) related to RMS value and maximum value, respectively, are defined as,

$$\tilde{I}_1=\frac{\tilde{f}}{\tilde{f}_0},\ \tilde{I}_2=\frac{\tilde{M}}{\tilde{M}_0},\ \tilde{I}_3=\frac{\tilde{x}_b}{\tilde{x}_{b0}},\ \tilde{I}_4=\frac{\tilde{x}_t}{\tilde{x}_{b0}} \tag{17}$$

$$I_1=\frac{f_{\max}}{f_{0,\max}},\ I_2=\frac{M_{\max}}{M_{0,\max}},\ I_3=\frac{x_{b,\max}}{x_{b0,\max}},\ I_4=\frac{x_{t,\max}}{x_{b0,\max}} \tag{18}$$

Table 2 Natural earthquake records used in numerical simulations

RSN	Event	Type	Year	Station	R_{jb} (km)	T_p (s)
169	Imperial Valley	Far field	1979	Delta	22.03	—
179	Imperial Valley	Near fault	1979	El Centro Array #4	4.90	4.788
1191	Chi-Chi	Far field	1999	CHY022	63.21	—
1511	Chi-Chi	Near fault	1999	TCU076	2.74	4.732

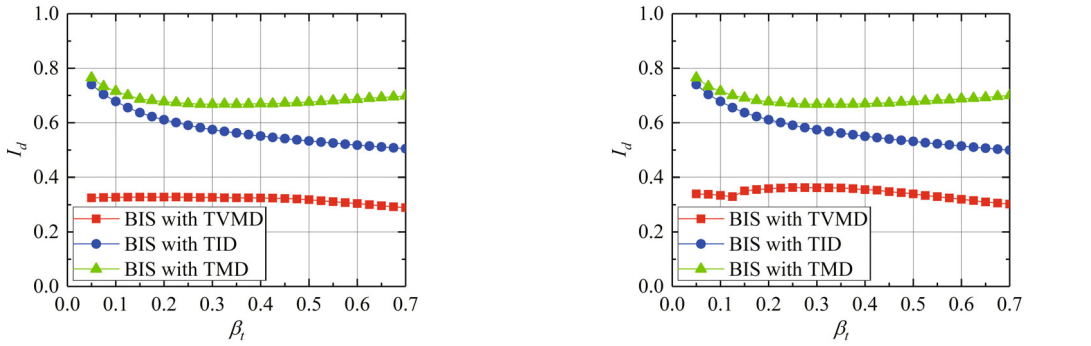

(a) Objective I_d obtained from η_{topt} and ξ_{topt} in Fig. 2 (b) Objective I_d obtained from η_{topt} and ξ_{topt} in Fig. 3

Fig. 5 Objective I_d

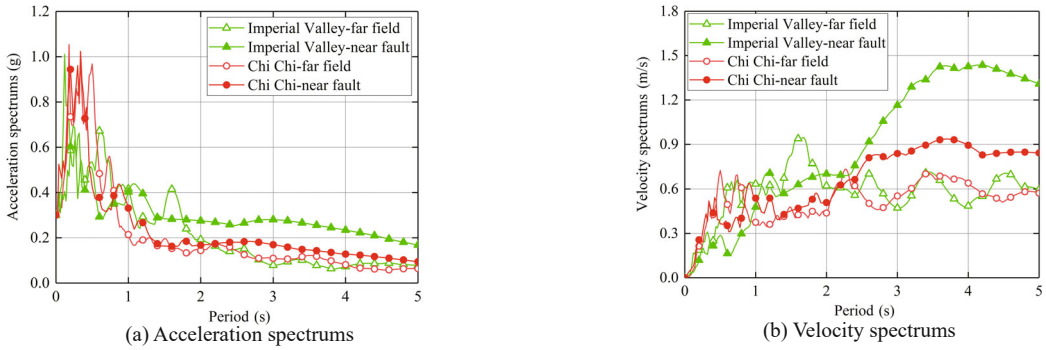

(a) Acceleration spectrums (b) Velocity spectrums

Fig. 6 Acceleration and velocity spectrums

where f_0, M_0 and x_{b0} are the seismic responses of the BIS without a control system, and the superscript ~ and subscript max represent the RMS value and maximum value, respectively. In this section, three mass ratios (β_t=0.05, 0.20 and 0.50) are considered for each control system, and the structural parameters of each control system are obtained based on the optimal design minimizing the base shear of the BIS in Section 3.2.

Tables 3 and 4 present the performance indices $\tilde{I}_i$ and I_i (i=1, 2, 3 or 4), respectively. It can be found from Tables 3 and 4 that the TVMD with a mass ratio β_t of 0.05 is very effective in reducing the RMS values of seismic response of the structural MDOF, which agrees well with the results obtained in Section 3. As the mass ratio β_t increases, the effectiveness of the TVMD does not change significantly in terms of RMS values under these earthquake records. However, it seems that the larger mass ratio (β_t=0.20 and 0.50) has an amplifying effect on the maximum base overturning moment under the Chi Chi-far field earthquake. With the increase of the mass ratio β_t, the effectiveness of the TID in terms of RMS and maximum values on mitigating the seismic response of

Table 3 Performance indices $\tilde{I}_i$ (i = 1,2, 3 and 4) in terms of RMS responses

Ground motion	Control system	β_t	$\tilde{I}_1$	$\tilde{I}_2$	$\tilde{I}_3$	$\tilde{I}_4$
Imperial Valley-far field RSN: 169 Uncontrolled $\tilde{f}_0 = 8.465\times10^6$ N $\tilde{M}_0 = 1.109\times10^8$ N·m $\tilde{x}_{b0} = 0.126$ m	TVMD	0.05	0.440	0.510	0.269	0.033
	TID	0.05	0.777	0.779	0.821	2.759
	TMD	0.05	0.780	0.782	0.844	3.278
	TVMD	0.20	0.435	0.593	0.268	0.040
	TID	0.20	0.542	0.551	0.599	1.241
	TMD	0.20	0.524	0.528	0.614	1.666
	TVMD	0.50	0.460	0.652	0.253	0.138
	TID	0.50	0.410	0.438	0.464	0.688
	TMD	0.50	0.396	0.402	0.505	1.092
Imperial Valley-near fault RSN: 179 Uncontrolled $\tilde{f}_0 = 2.550\times10^7$ N $\tilde{M}_0 = 3.329\times10^8$ N·m $\tilde{x}_{b0} = 0.379$ m	TVMD	0.05	0.325	0.324	0.233	0.021
	TID	0.05	0.709	0.710	0.740	2.594
	TMD	0.05	0.718	0.719	0.765	2.964
	TVMD	0.20	0.320	0.309	0.234	0.022
	TID	0.20	0.496	0.497	0.552	1.173
	TMD	0.20	0.497	0.498	0.574	1.553
	TVMD	0.50	0.317	0.307	0.218	0.064
	TID	0.50	0.346	0.348	0.417	0.638
	TMD	0.50	0.363	0.364	0.458	0.985
Chi Chi-far field RSN: 1191 Uncontrolled $\tilde{f}_0 = 5.971\times10^6$ N $\tilde{M}_0 = 7.940\times10^7$ N·m $\tilde{x}_{b0} = 0.089$ m	TVMD	0.05	0.498	0.655	0.344	0.035
	TID	0.05	0.702	0.717	0.706	2.215
	TMD	0.05	0.701	0.713	0.725	2.425
	TVMD	0.20	0.491	0.827	0.334	0.045
	TID	0.20	0.582	0.612	0.608	1.133
	TMD	0.20	0.611	0.622	0.692	1.702
	TVMD	0.50	0.487	0.706	0.321	0.121
	TID	0.50	0.484	0.558	0.543	0.775
	TMD	0.50	0.513	0.520	0.677	1.481
Chi Chi-near fault RSN: 1511 Uncontrolled $\tilde{f}_0 = 9.558\times10^6$ N $\tilde{M}_0 = 1.250\times10^7$ N·m $\tilde{x}_{b0} = 0.142$ m	TVMD	0.05	0.415	0.461	0.277	0.029
	TID	0.05	0.729	0.731	0.759	2.561
	TMD	0.05	0.725	0.726	0.772	2.921
	TVMD	0.20	0.406	0.536	0.278	0.034
	TID	0.20	0.552	0.557	0.597	1.184
	TMD	0.20	0.568	0.570	0.665	1.759
	TVMD	0.50	0.406	0.488	0.260	0.098
	TID	0.50	0.447	0.462	0.532	0.802
	TMD	0.50	0.445	0.448	0.591	1.323

the structural MDOF increases, and its stroke decreases. Considering the stroke of the TID for installation, it is recommended that the mass ratio β_t is greater than 0.20.

Figures 7 and 8 present the time histories of two typical responses under the action of the Imperial Valley-far field earthquake and Imperial Valley-near fault earthquake, respectively. The two responses are the relative displacement between the base isolation floor and the foundation and the strokes of three control systems. In Figs. 7 and 8, the mass ratios for the TVMD, TID and TMD are, respectively, 0.05, 0.20 and 0.20. It can be seen from Fig. 7 that the structural responses under the near fault earthquake are significantly greater than those under the far field earthquake, and it seems that the TVMD is more efficient in reducing the seismic response than the TID and TMD with a lower mass ratio and a smaller stroke.

For the Imperial Valley-far field earthquake, it can be found from Fig. 7(a) that there is a large response after the 60th second, and before that, the efficiency of the three control systems is low. For the Imperial Valley-near fault earthquake, the isolation floor has a large

Table 4 Performance indices I_i (i=1, 2, 3 and 4) in terms of maximum responses

Ground motion	Control system	β_t	I_1	I_2	I_3	I_4
Imperial Valley-far field RSN:169 Uncontrolled f_0= 2.692×10^7 N M_0= 3.529×10^8 N·m x_{b0}= 0.401 m	TVMD	0.05	0.525	0.657	0.279	0.050
	TID	0.05	0.727	0.723	0.764	2.515
	TMD	0.05	0.737	0.730	0.788	3.069
	TVMD	0.20	0.518	0.623	0.284	0.062
	TID	0.20	0.495	0.525	0.568	1.116
	TMD	0.20	0.494	0.487	0.586	1.626
	TVMD	0.50	0.612	0.681	0.275	0.232
	TID	0.50	0.379	0.461	0.450	0.671
	TMD	0.50	0.387	0.381	0.485	1.071
Imperial Valley-near fault RSN:179 Uncontrolled f_0= 6.592×10^7 N M_0= 8.700×10^8 N·m x_{b0}= 0.981 m	TVMD	0.05	0.541	0.586	0.385	0.040
	TID	0.05	0.913	0.916	0.912	2.558
	TMD	0.05	0.914	0.915	0.938	2.787
	TVMD	0.20	0.493	0.540	0.387	0.045
	TID	0.20	0.694	0.696	0.728	1.407
	TMD	0.20	0.737	0.739	0.803	1.839
	TVMD	0.50	0.572	0.672	0.363	0.148
	TID	0.50	0.530	0.537	0.575	0.836
	TMD	0.50	0.585	0.578	0.726	1.307
Chi Chi-far field RSN:1191 Uncontrolled f_0= 1.981×10^7 N M_0= 2.943×10^8 N·m x_{b0}= 0.295 m	TVMD	0.05	0.716	0.892	0.438	0.052
	TID	0.05	0.793	0.787	0.810	2.691
	TMD	0.05	0.817	0.799	0.859	2.610
	TVMD	0.20	0.673	1.155	0.432	0.067
	TID	0.20	0.765	0.773	0.797	1.407
	TMD	0.20	0.764	0.712	0.845	2.300
	TVMD	0.50	0.719	1.061	0.396	0.170
	TID	0.50	0.665	0.739	0.736	1.092
	TMD	0.50	0.685	0.629	0.792	2.069
Chi Chi-near fault RSN:1511 Uncontrolled f_0= 3.639×10^7 N M_0= 4.726×10^8 N·m x_{b0}= 0.540 m	TVMD	0.05	0.714	0.747	0.419	0.059
	TID	0.05	0.955	0.942	0.950	2.269
	TMD	0.05	0.950	0.947	0.973	2.538
	TVMD	0.20	0.635	0.765	0.425	0.070
	TID	0.20	0.810	0.823	0.828	1.312
	TMD	0.20	0.837	0.826	0.909	1.740
	TVMD	0.50	0.703	0.878	0.381	0.179
	TID	0.50	0.635	0.656	0.667	0.885
	TMD	0.50	0.688	0.687	0.807	1.373

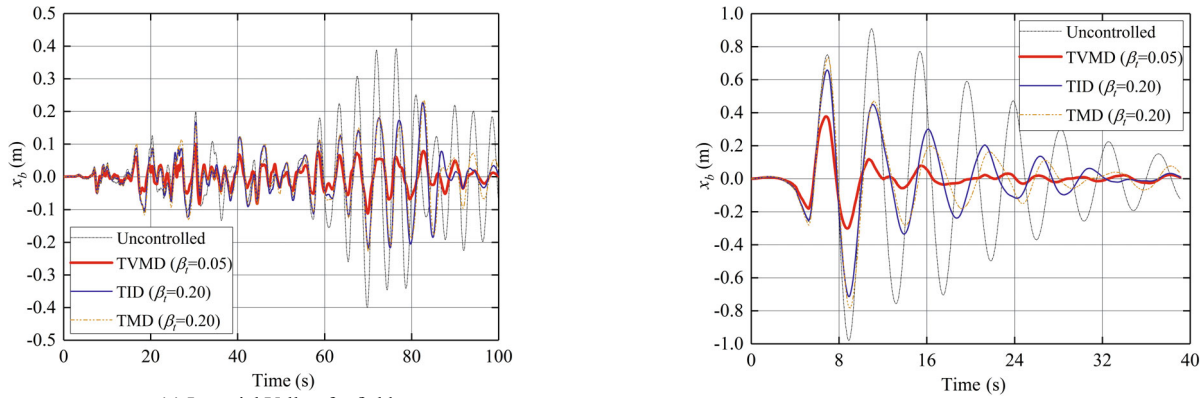

(a) Imperial Valley-far field (b) Imperial Valley-near fault

Fig. 7 Relative displacement between base isolation floor and foundation

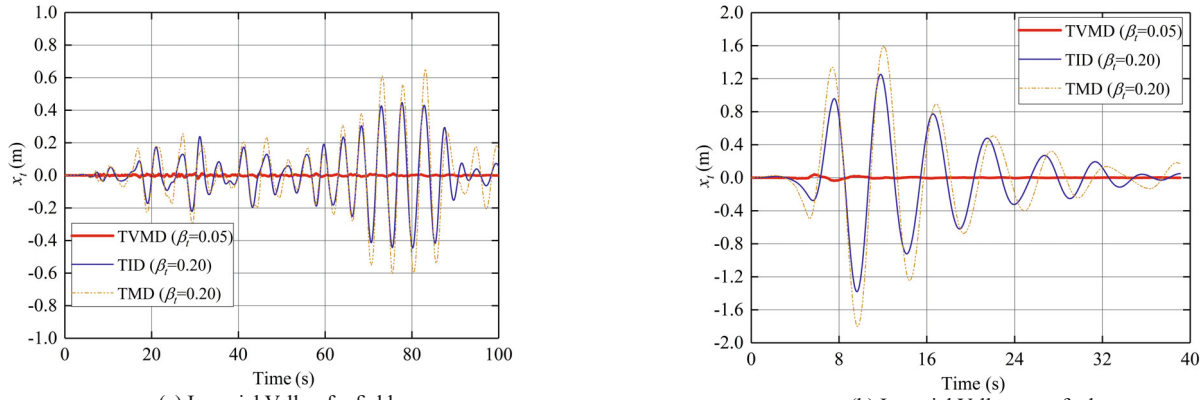

(a) Imperial Valley-far field (b) Imperial Valley-near fault

Fig. 8 Strokes of the three control systems

seismic response in a short time due to the velocity pulse, as shown in Fig. 7(b). It appears that the TVMD plays a great role in reducing structural responses in the first oscillation cycle of this earthquake, which means that the TVMD has the best activation sensitivity compared to TID and TMD. The reason for this may be that the optimal stiffness and the optimal damping coefficient of the TVMD are relatively larger than those of the TID and TMD.

5 Concluding remarks

The effects of three control systems, TVMD, TID and TMD, combined with base isolation on the seismic responses, including the base shear, base overturning moment, and relative displacement between the base isolation floor and the foundation, were systematically studied. The optimal designs of these three control systems were carried out by using three different objectives based on a BIS subjected to white noise stochastic ground motion. The results show that the three control systems were all effective in minimizing the root mean square value of seismic responses, including the base shear of the BIS, the absolute acceleration of structural SDOF, and the relative displacement between the base isolation floor and the foundation. By considering the superstructure as a structural MDOF, a series of time history analyses were performed to investigate the effectiveness and activation sensitivity of the three control systems under far field and near fault seismic excitations. The results show that the effectiveness of TID and TMD with optimized parameters on mitigating the seismic responses of base isolated structures increased as the mass ratio increased, and the effectiveness of TID was always better than TMD with the same mass ratio. The TVMD with a lower mass ratio was more efficient in reducing the seismic response than the TID and TMD. Furthermore, the TVMD, when compared with the TMD and TID, had better activation sensitivity and smaller stroke. The optimal designs of TVMD, TID and TMD, in this study, were carried out by considering the stochastic ground motion as a white Gaussian noise random process, while a reliability-based design optimization will be conducted in a future work. Furthermore, experimental investigations of the new control technology are required.

Acknowledgement

This project was supported by the National Key Research and Development Program of China (Grant Nos. 2017YFC0703600 and 2017YFC0703604).

References

Adam C, Matteo AD, Furtmüller T and Pirrotta A (2017), "Earthquake Excited Base-Isolated Structures Protected by Tuned Liquid Column Dampers: Design Approach and Experimental Verification," *Procedia Engineering*, **199**: 1574–1579.

Arai T, Aburakawa T, Ikago K, Hori N and Inoue N (2009), "Verification on Effectiveness of a Tuned Viscous Mass Damper and Its Applicability to Non-Linear Structural Systems," *Journal of Structural and Construction Engineering*,**74**(645): 1993–2002.

Chen MZ, Hu Y, Huang L and Chen G (2014), "Influence of Inerter on Natural Frequencies of Vibration Systems," *Journal of Sound and Vibration*, **333**(7): 1874–1887.

De Domenico D and Ricciardi G (2018a), "An Enhanced Base Isolation System Equipped with Optimal Tuned Mass Damper Inerter (TMDI)," *Earthquake Engineering and Structural Dynamics*, **47**(5): 1169–1192.

De Domenico D and Ricciardi G (2018b), "Optimal Design and Seismic Performance of Tuned Mass Damper Inerter (TMDI) for Structures with Nonlinear Base Isolation Systems," *Earthquake Engineering and Structural Dynamics*, **47**(12): 2539–2560.

Giaralis A and Petrini F (2017), "Wind-Induced Vibration Mitigation in Tall Buildings Using the Tuned Mass Damper Inerter," *Journal of Structural Engineering*, **143**(9): 04017127.

Hashimoto T, Fujita K, Tsuji M and Takewaki I (2015), "Innovative Base-isolated Building with Large Mass-Ratio TMD at Basement for Greater Earthquake Resilience," *Future Cities and Environment*, **1**: 9.

Hu Y and Chen MZ (2015), "Performance Evaluation for Inerter-based Dynamic Vibration Absorbers," *International Journal of Mechanical Sciences*, **99**: 297–307.

Huang ZW, Hua XG, Chen ZQ and Niu HW (2019), "Optimal Design of TVMD with Linear and Nonlinear Viscous Damping for SDOF Systems Subjected to Harmonic Excitation," *Structural Control and Health Monitoring*, **26**(10): e2413.

Ikago K, Saito K and Inoue N (2012), "Seismic Control of Single Degree of Freedom Structure Using Tuned Viscous Mass Damper," *Earthquake Engineering and Structural Dynamics*, **41**(3): 453–474.

Jangid RS and Banerji P (1998), "Effects of Isolation Damping on Stochastic Response of Structures with Nonlinear Base Isolators," *Earthquake Spectra*, **14**(1): 95–114.

Kawamata S (1973), "Development of a Vibration Control System of Structures by Means of Mass Pumps," Institute of Industrial Science, University of Tokyo: Tokyo.

Kelly JM (1999), "The Role of Damping in Seismic Isolation," *Earthquake Engineering and Structural Dynamics*, **28**(1): 3–20.

Lazar IF, Neild SA and Wagg DJ (2014), "Using an Inerter-based Device for Structural Vibration Suppression," *Earthquake Engineering and Structural Dynamics*, **43**(8): 1129–1147.

Lee JJ and Kelly JM (2019), "The Effect of Damping in Isolation System on the Performance of Base-Isolated System," *Journal of Rubber Research*, 1–13.

Li YF, Li SY, Wang JZ and Chen ZQ (2020a), "A New Type of Damper Combining Eddy Current Damping with Rack and Gear," *Journal of Vibration and Control*, (1): 107754632098711.

Li SY, Li YF, Wang JZ and Chen ZQ (2020b), "Theoretical Investigations on the Linear and Nonlinear Damping Force for an Eddy Current Damper Combining with Rack and Gear," *Journal of Vibration and Control*, 107754632098778.

Liu X, Jiang JZ, Titurus B and Harrison A (2018), "Model Identification Methodology for Fluid-Based Inerter," *Mechanical Systems and Signal Processing*, **106**: 479–494.

Lu X, Wang D and Wang S (2016), "Investigation of the Seismic Response of High-Rise Buildings Supported on Tension-Resistant Elastomeric Isolation Bearings," *Earthquake Engineering and Structural Dynamics*, **45**(13): 2207–2228.

Marian L and Giaralis A (2014), "Optimal Design of a Novel Tuned Mass Damper Inerter (TMDI) Passive Vibration Control Configuration for Stochastically Support-Excited Structural Systems," *Probabilistic Engineering Mechanics*, **38**: 156–164.

Marian L and Giaralis A (2017), "The Tuned Mass Damper Inerter for Harmonic Vibrations Suppression, Attached Mass Reduction, and Energy Harvesting," *Smart Structures and Systems*, **19**(6): 665–678.

Nakaminami S, Kida H, Ikago K and Inoue N (2011), "Application of Viscous Mass Damper with Force Restriction Mechanism to Base-Isolated Structures and Its Effectiveness," *Journal of Structural and Construction Engineering*, **76**(670): 2077–2086.

Nepal S and Saitoh M (2020), "Improving the Performance of Conventional Base Isolation Systems by an External Variable Negative Stiffness Device Under Near-Fault and Long-Period Ground Motions," *Earthquake Engineering and Engineering Vibration*, **19**(4): 985–1003.

Papageorgiou C and Smith MC (2005), "Laboratory Experimental Testing of Inerters," *Proceedings of the 44th IEEE Conference on Decision and Control*, IEEE, 3351–3356.

Peng YB, Ma YY, Huang TC and De Domenico D (2020), "Reliability-Based Design Optimization of Adaptive Sliding Base Isolation System for Improving Seismic Performance of Structures," *Reliability Engineering and System Safety*, (205): 107167.

Pietrosanti D, De Angelis M and Basili M (2017), "Optimal Design and Performance Evaluation of Systems with Tuned Mass Damper Inerter (TMDI)," *Earthquake Engineering and Structural Dynamics*, **46**(8): 1367–1388.

Qiu C and Tian L (2018), "Feasibility Analysis of SMA-Based Damping Devices for Use in Seismic Isolation of Low-Rise Frame Buildings," *International Journal of Structural Stability and Dynamics*, **18**(6): 1850087.

Rezazadeh H, Amini F and Afshar MA (2020), "Effect of Inertia Nonlinearity on Dynamic Response of an Asymmetric Building Equipped with Tuned Mass Dampers," *Earthquake Engineering and Engineering Vibration*, **19**(2): 499–513.

Ryan KL and Polanco J (2008), "Problems with Rayleigh Damping in Base-Isolated Buildings," *Journal of Structural Engineering*, **134**(11): 1780–1784.

Satish B and Anil CW (2017), "Seismic Response Evaluation of Base-Isolated Reinforced Concrete Buildings Under Bidirectional Excitation," *Earthquake Engineering and Engineering Vibration*, **16**(2): 365–382.

Smith MC (2002), "Synthesis of Mechanical Networks: the Inerter," *IEEE Transactions on Automatic Control*, **47**(10): 1648–1662.

Sun H, Zuo L, Wang X, Peng J and Wang W (2019), "Exact H_2 Optimal Solutions to Inerter-based Isolation Systems for Building Structures," *Structural Control and Health Monitoring*, **26**(6): e2357.

Taniguchi T, Der Kiureghian A and Melkumyan M (2008), "Effect of Tuned Mass Damper on Displacement Demand of Base-Isolated structures," *Engineering Structures*, **30**(12): 3478–3488.

Walsh KK and Abdullah MM (2006), "Adaptive Base-isolation of Civil Structures Using Variable Amplification," *Earthquake Engineering and Engineering Vibration*, **5**(2): 223–233.

Wen Y, Chen Z and Hua X (2016), "Design and Evaluation of Tuned Inerter-based Dampers for the Seismic Control of MDOF Structures," *Journal of Structural Engineering*, **143**(4): 04016207.

Xiang P and Nishitani A (2014), "Optimum Design for More Effective Tuned Mass Damper System and Its Application to Base-Isolated Buildings," *Structural Control and Health Monitoring*, **21**(1): 98–114.

Xu K, Bi K, Han Q, Li, X and Du X (2019), "Using Tuned Mass Damper Inerter to Mitigate Vortex-Induced Vibration of Long-span Bridges: Analytical Study," *Engineering Structures*, **182:** 101–111.

Xue SD, Shan MY, Li XY, Liang SZ, Huang FY and Liu Y (2019), "Shaking Table Test and Numerical Simulation of an Isolated Cylindrical Latticed Shell Under Multiple-Support Excitations," *Earthquake Engineering and Engineering Vibration*, **18**(3): 611–630.

Yang JN, Danielians A and Liu SC (1991), "Aseismic Hybrid Control Systems for Building Structures," *Journal of Engineering Mechanics*, **117**(4): 836–853.

Ye K, Shu S, Hu L and Zhu H (2019), "Analytical Solution of Seismic Response of Base-Isolated Structure with Supplemental Inerter," *Earthquake Engineering and Structural Dynamics*, **48**(9): 1083–1090.

Zhang R, Zhao Z, Pan C, Ikago K and Xue S (2020), "Damping Enhancement of Inerter System," *Structural Control and Health Monitoring*, e2523.

Zhao Z, Chen Q, Zhang R, Pan C and Jiang Y (2019a), "Optimal Design of an Inerter Isolation System Considering the Soil Condition," *Engineering Structures*, **196**: 109324.

Zhao Z, Zhang R, Jiang Y and Pan C (2019b), "Seismic Response Mitigation of Structures with a Friction Pendulum Inerter System," *Engineering Structures*, **193**: 110–120.